The International Journal of Advanced Manufacturing Technology (2024) 130:5951–5964
https://doi.org/10.1007/s00170-023-12937-2

ORIGINAL ARTICLE

A comparative study of the thermal and mechanical cutting influence on the cut-edge hardness of structural steels S355 and S1100

Paul Diekhoff[1] · Jiamin Sun[1] · Thomas Nitschke-Pagel[1] · Klaus Dilger[1]

Received: 21 August 2023 / Accepted: 28 December 2023 / Published online: 30 January 2024

Abstract
Thermal and mechanical cutting processes are commonly applied in manufacturing industries for making a specific size and shape of samples. The material properties of the heat-affected metal at the cut edge might be different from those of the parent metal. Hardness as a very important parameter for the assessment of material properties has been widely used in the design procedure. The Vickers hardness test is a versatile method to measure material hardness in practice. In this study, a comparison of cut-edge hardness between the thermal and mechanical cutting processes was performed on the structural steels S355 and S1100 by using the Vickers hardness test method with a small angle at cut edges to widen the heat-affected zone (HAZ). Based on the measurements, the influence of the Vickers test load on the magnitude and distribution of cut-edge hardness for laser-cut samples of steels S355 and S1100 was clarified. Furthermore, the effects of cutting processes on the hardness were illustrated. Finally, a comparison between the distribution characteristics of the cut-edge hardness of steels S355 and S1100 was made. For structural steel, it is recommended to apply the Vickers hardness testing method with a test load of 1 kpf and with a small angle at cut edges to widen the HAZ and to get reasonable results. The hardness distribution and the maximum for laser- and plasma-cut edges are similar, depending on the material, with a maximum of 450 HV1 for S355N and of 550 HV1 for S1100M.

Keywords Cutting processes · Hardness · Structural steels · Vickers hardness test

1 Introduction

Structural steel S355 has been widely used in the construction, bridge, and ship industry because of its predominant strength characteristics [1]. Over the recent decades, to meet the massive increase in the demand for fuel economy and environmental protection, lightweight materials such as ultra-high-strength steel S1100 have been developed and increasingly applied in manufacturing industries to reduce the production weight [2, 3]. For fabrication and assembly in the industry, cutting processes consisting of thermal and mechanical cutting are usually used for producing a specific shape and size of the components [4]. When structural steel is cut by using thermal cutting processes, a heat-affected zone (HAZ) is generated at the cut edge [5]. The microstructure of HAZ is different compared to that of the base metal (BM), which affects the magnitude and distribution of hardness [6]. It is well known that hardness is commonly taken as a very important parameter to estimate the mechanical properties of materials such as fatigue strength and fracture toughness [7]. Therefore, it is necessary to know the magnitude and distribution of hardness at the cut edge of structural steel in the design procedure precisely.

Currently, four typical test methods, namely Rockwell, Brinell, Knoop, and Vickers hardness testing, are applied in practice [8]. Among these methods, Vickers hardness testing

✉ Paul Diekhoff
p.diekhoff@tu-bs.de

✉ Jiamin Sun
jiamin.sun@tu-bs.de

Thomas Nitschke-Pagel
t.pagel@tu-bs.de

Klaus Dilger
k.dilger@tu-bs.de

[1] Institute of Joining and Welding Technology, Technische Universität Braunschweig, Langer Kamp 8, 38106 Braunschweig, Germany

is mainly used in practice because it is easy to apply and can be used for all kinds of metals. From the standpoint of processes, the thermal cutting process is similar to the welding process [9]. Sokolov et al. [10] studied the magnitude and distribution of hardness in thick plate S355 steel weldments induced by laser welding. They found that the hardness in HAZ increases from 190–200 to 450–500 HV5 in BM. This is also seen in [11] by Dunder et al. for the steel P92. Waterschoot et al. [12] and Farabi et al. [13] investigated the magnitude and distribution of the microindentation hardness of laser-welded high-strength dual-phase (DP) steel joints. They pointed out that a softened zone with lower hardness in the outer HAZ exists, and the softening degree is related to the heat input and strength grade of BM. Boujelbene et al. [14] studied the influence of laser cutting parameters on the magnitude of microhardness in the HAZ of mid-hardened C45 steel. They showed that the mean magnitude of microhardness in HAZ increases with increasing laser power and cutting speed. Lazarevie and Lazarevie [15] measured the hardness distribution in the HAZ of X6CrNiMoTi 17-12-2 steel induced by plasma cutting. They found out that the microhardness in the HAZ increases compared to the BM hardness due to the change in the grain size.

Although tremendous research has investigated the magnitude and distribution of hardness in cut steel plates comparing the influence of the quality and fatigue strength (e.g., [IIW19,IIW20]), there have been few works comparing the distribution characteristics of hardness in cut samples of different structural steel grades. Furthermore, it is still unclear whether the cutting processes influence the magnitude and distribution of the cut-edge hardness of structural steel. Besides, there has almost been no guidance on the determination of the Vickers test load for measuring hardness at cut edges [16].

In the current work, thermal (laser and plasma) and mechanical (by milling) cutting were utilized to produce specimens of steels S355 and S1100. The microstructure was characterized in terms of macrographs and micrographs, and the cut-edge hardness was measured and analyzed. This research shows a comparison of the test load at cut edges and a detailed characterization of the boundary layer in the case of hardness distribution for different cutting methods. It gives guidance to apply the Vickers hardness testing method with a small angle at cut edges to widen the HAZ and to get reasonable results with a test load of HV1.

2 State of the art

2.1 Vickers hardness testing

The Vickers hardness test is commonly applied to determine hardness in industry, which is an appropriate method for a broad range of materials. Figure 1 schematically illuminates the theory of Vickers hardness testing [17]. The surface of the material is indented by a diamond indenter with a load (F) for a few seconds (10 to 15 s). After the removal of the load, two diagonals of the indentation are left on the surface of the material as seen in Fig. 1. The lengths of the two diagonals, d_1 and d_2 in Fig. 1, can be measured by using a microscope and their average (d) can be calculated by using Eq. 1. The value of the Vickers hardness at a point on the surface of the material can be determined by using Eq. 2.

$$d = \frac{d_1 + d_2}{2} \tag{1}$$

$$HV = \frac{2F \sin \frac{136^\circ}{2}}{d^2} \tag{2}$$

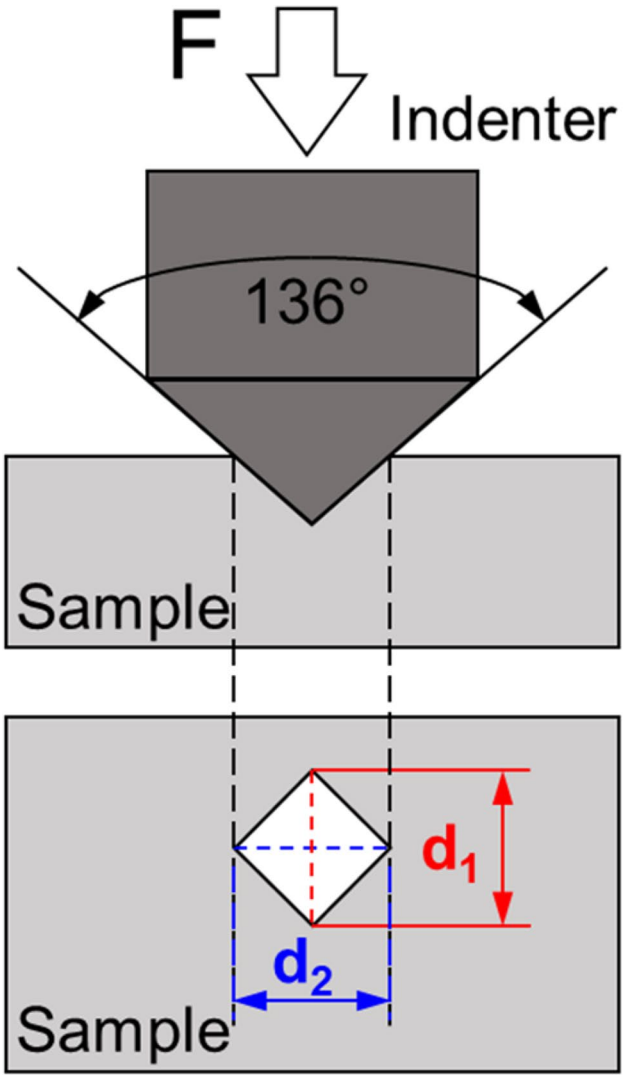

Fig. 1 Schematic illustration of the Vickers hardness test. From [17]

where F is the load in kilograms-force; d is the mean value of d_1 and d_2 in millimeters. It is well known that the Vickers hardness test has a wide range of applied loads, which can be used to measure both the macro- and microhardness of materials as seen in Fig. 2 [18]. With the variation in the load F, the length of the diagonal is changed accordingly. Obviously, the length (d_1, d_2, and d) is proportional to the load F. From Fig. 2, it can be seen that the number of grains in the area of the indentation increases with the load F. If the material consists of a few different phases, the phase fractions at this area could also be changed with the load F.

2.2 Cutting processes

To date, numerous cutting processes have been developed, which can be categorized into two groups. One includes thermal cutting techniques like beam cutting, arc cutting, and oxygen cutting [19], and the other group uses mechanical cutting techniques like waterjet cutting, milling, and diamond-saw cutting [20].

In the present study, the commonly used thermal (laser and plasma) and mechanical (milling) cutting in manufacturing industries are briefly introduced as shown in Fig. 3. The laser cutting utilizes a focused high–power density laser beam to melt material in a localized area as seen in Fig. 3a [21]. A co-axial gas jet is applied to blow off the molten material and to create a kerf. The plasma cutting process utilizes a high-energy stream of plasma (ionized gas) as its heat source as shown in Fig. 3b [22], which is directed to heat and melt the workpiece with extremely high speed and temperature. Then, the compressed plasma and shield gas blows away the hot molten material, resulting in the separation of the workpiece. In milling, a round tool is moved around the sheet to be machined, producing the final contour in several steps as seen in Fig. 3c [23].

From the above description, one can see that the processing mechanism of thermal (laser and plasma) cutting is similar. The material is melted by using a heat source and then blown away to separate the workpiece by using the thermal cutting process. However, thermal and mechanical cutting are completely different in essence.

2.3 Sub-zones of the heat-affected zone

The HAZ is generated at the cut edge induced by thermal cutting, which often consists of four zones: the coarse-grained HAZ (CGHAZ), the fine-grained HAZ (FGHAZ), the inter-critical HAZ (ICHAZ), and the sub-critical HAZ (SCHAZ) adjacent to the BM [24]. The temperature ranges of these zones in structural steels are 1100 °C, melting temperature ($T_{melting}$); A_{c3}, 1100 °C; A_{c1}–A_{c3}; and 650 °C, A_{c1} [25]. The values of A_{c1} and A_{c3} can be determined by using Eqs. 3 and 4 as seen below:

$$A_{c1} = 723 - 10.7\text{Mn} - 16.9\text{Ni} + 29\text{Si} + 16.9\text{Cr} + 290\text{As} + 6.4\text{W} \tag{3}$$

$$A_{c3} = 912 - 200\sqrt{\text{C}} - 15.2\text{Ni} + 44.7\text{Si} + 315\text{Mo} + 13.1\text{W} - (30\text{Mn} + 11\text{Cr} + 20\text{Cu} - 700\text{P} - 400\text{Al} - 120\text{As} - 400\text{Ti}) \tag{4}$$

Figure 4 shows schematically the variation in microstructure in the HAZ of structural steels [26]. From Fig. 4, it can be seen that the parent phase of BM in the CGHAZ and FGHAZ transfers to austenite during heating. The finally generated microstructure during cooling is related to the cooling rate $\Delta t_{8/5}$ and continuous-cooling-transformation (CCT) diagram. The $\Delta t_{8/5}$ time is the representative period in which the melt and HAZ cools down from 800 to 500 °C. The partial initial phase in the ICHAZ would transform during thermal processes. In the SCHAZ, the parent phase does not transform during heating. Nevertheless, the parent phase would be over-tempered during cooling if it is the martensite or auto-tempered martensite. Otherwise, it would not be changed anymore. In other words, no SCHAZ exists for the heat-affected material where the parent phase of BM is not martensite or auto-tempered martensite.

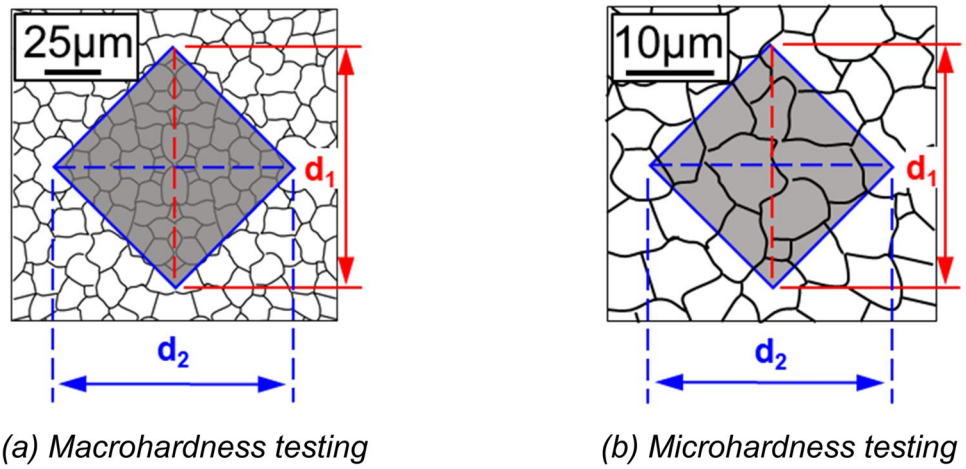

(a) Macrohardness testing (b) Microhardness testing

Fig. 2 Schematic indentation hardness of a polycrystalline material ($F_a > F_b$). From [17]

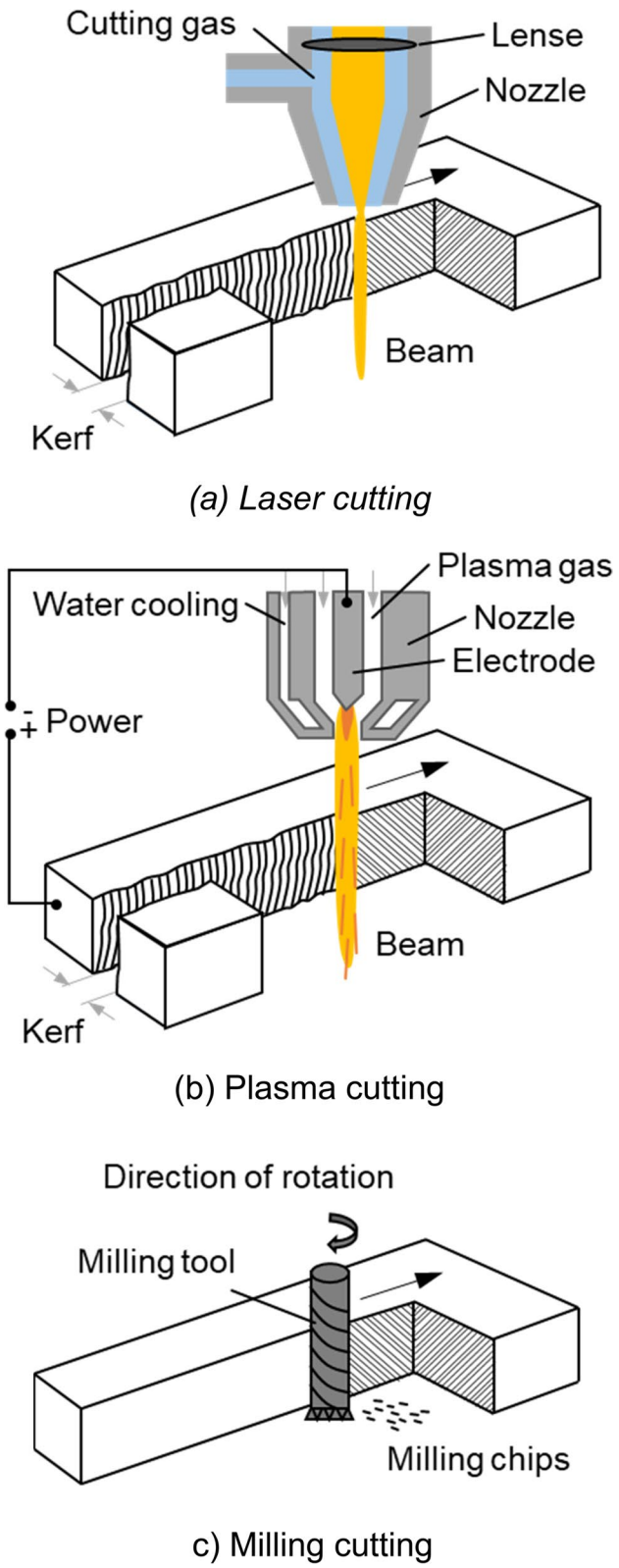

Fig. 3 Schematic illustration of the cutting method

Many studies showed that the width of HAZ is very narrow induced by thermal cutting processes [27, 28]. It can be expected that it is not easy to catch the distribution characteristics of hardness at the cut edge by using the experimental method. To solve this problem, a method was used that a wider width of HAZ could be obtained by taking the cross section with a small angle such as 5 ° used in this study as shown in Fig. 5.

This research is intended to contribute to a wise application of hardness measurement methods on thermal cutting edges in order to avoid the hardness distribution not being correctly determined. The following objectives are pursued in this work: What is the best test load for determining the hardness of thermal cutting edges and how do the hardness distributions differ over the sheet thickness and between different cutting processes?

3 Experimental procedure

In this study, the structural steels S355NC and S1100M were investigated. The measured chemical compositions of both steels S355N and S1100M are listed in Tables 1 and 2, respectively. In the current work, laser, plasma, and mechanical cutting processes were used. The dimensions of the cut samples are shown in Fig. 6. Note that the sizes of the cut specimens of steels S355NC and S1100M are the same except for the plate thickness. The plate thickness of S355NC steel is 8 mm and that of S1100M steel is 7 mm. The applied cutting process parameters can be seen in Tables 3, 4, and 5. Initially, thermocouples were arranged on the bottom surface of the workpiece for measuring the $\Delta t_{8/5}$ time. The locations of the thermocouples can be seen in Table 6. After the thermal and mechanical cutting processes, the microstructures were observed by using an optical microscope. Furthermore, the hardness along line 1, line 2, and line 3 as seen in Figs. 5 and 7 was measured. The measurements were carried out on a stationary universal hardness testing machine ZHV30 according to the Vickers method (DIN EN ISO 6507-1) with different test loads; see Fig. 8. In the present work, the experimental plan is summarized as seen in Table 7.

4 Experimental results and discussion

4.1 Microstructures

Figure 9 shows the related macro- and micrographs at the transverse mid-cross section of mechanically cut specimens of steels S355NC and S1100M. Figure 9 illustrates in expectance

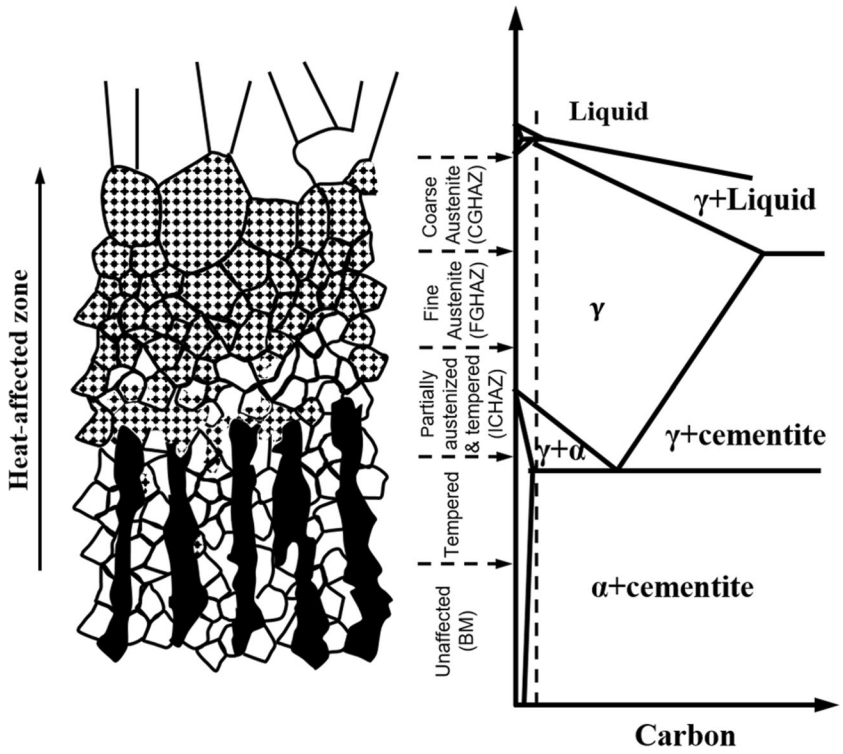

Fig. 4 Schematic illumination of microstructural variation in the HAZ of structural steels. From [26]

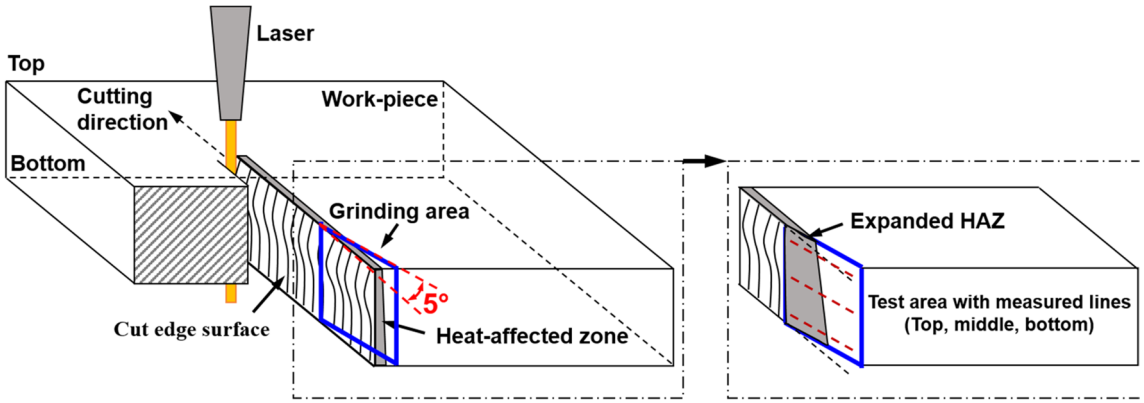

Fig. 5 Schematic illustration of obtaining a wider width of HAZ. Refer to [29]

Table 1 Measured chemical composition of S355NC steel, wt%

Elements	C	Si	Mn	P	S	W	Cu
Value	0.148	0.206	1.4	0.0118	0.0022	<0.005	0.0097
Elements	Mo	Ni	Al	Ti	Cr	As	Fe
Value	0.0052	0.0185	0.0324	0.0011	0.0331	0.0148	Balance

Table 2 Measured chemical composition of S1100M steel, wt%

Elements	C	Si	Mn	P	S	W	Cu
Value	0.175	0.269	1.43	0.0087	0.001	<0.005	0.443
Elements	Mo	Ni	Al	Ti	Cr	As	Fe
Value	0.395	0.977	0.0479	0.0194	0.722	0.014	Balance

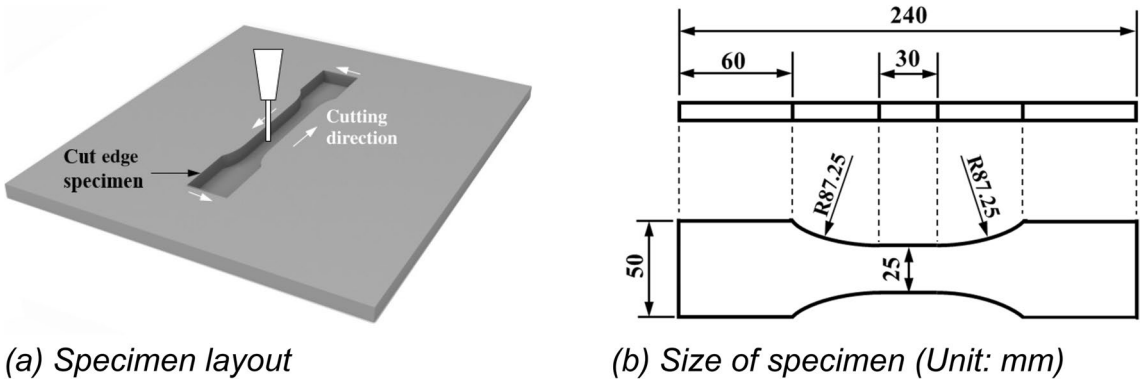

Fig. 6 **a** Layout and **b** sizes of cut specimens (unit: mm) of structural steels S355NC and S1100M

Table 3 Laser cutting process parameters

Parameters	Materials	Power (W)	Cutting speed (m/min)	Protection gas	Gas pressure (MPa)	Standoff distance (mm)
Values	S355NC/S1100M	5000	2.65	O_2	0.5	1

Table 4 Plasma cutting process parameters

Parameters	Materials	Plasma arc current (A)	Plasma arc voltage (V)	Cutting speed (m/min)	Plasma gas (bar)	Swirl gases (bar)	Standoff distance (mm)
Values	S355NC/S1100M	60	131	2.2	8.0 O_2	1.7 O_2, 4.0 air	2

Table 5 Mechanical cutting process—milling parameters

Parameters	Materials	Rotation speed (1/min)	Cutting speed (m/min)	Feed rate (mm/min)	Milling cutter diameter	Toothfeed (mm/tooth/rotation)
Values	S355NC/S1100M	2600	130	234	Ø 16	0.03

Table 6 Locations of thermocouples

Materials	Number	Distance to the cut edge (mm)
S355NC	TC-1	0.27
S1100M	TC-2	0.35

that no HAZ is generated at the cut edge independent from the material, because the peak temperature at the cut edge during mechanical cutting is very low [30]. In Fig. 9, one can see that the initial phase of S355NC steel is ferrite-pearlite and that of S1100M steel is tempered martensite. Figures 10 and 11 display the macro- and micrographs of laser- and plasma-cut specimens, respectively. Figures 10 and 11 show the HAZ is generated by laser and plasma cutting of steels S355NC and S1100M. Independent from the cutting process, the initial phase of the steel S355NC (ferrite-pearlite) transforms to martensite in HAZ, while that of S1100M (auto-tempered martensite) converts to martensite in HAZ. This is due to the very high cooling speed during thermal cutting as seen in Fig. 12. From Fig. 10, a very interesting phenomenon can be found that the width of HAZ at the top side is narrower than that at the bottom side in the laser-cut specimens of both steels S355NC and S1100M, which is obviously opposite to the width of HAZ along the plate thickness direction in the laser-welded joints. This is because the melted material at the top side is blown down by the protection gas through the bottom area during laser cutting, which causes the bottom heat-affected material to endure a longer high-temperature time. Comparing Fig. 10 to Fig. 11, one can see that the width of HAZ is very homogeneous through the plate thickness direction in the plasma-cut samples of both steels S355NC and S1100M. This is due to the gas pressure (from compressed plasma and shield gas) which

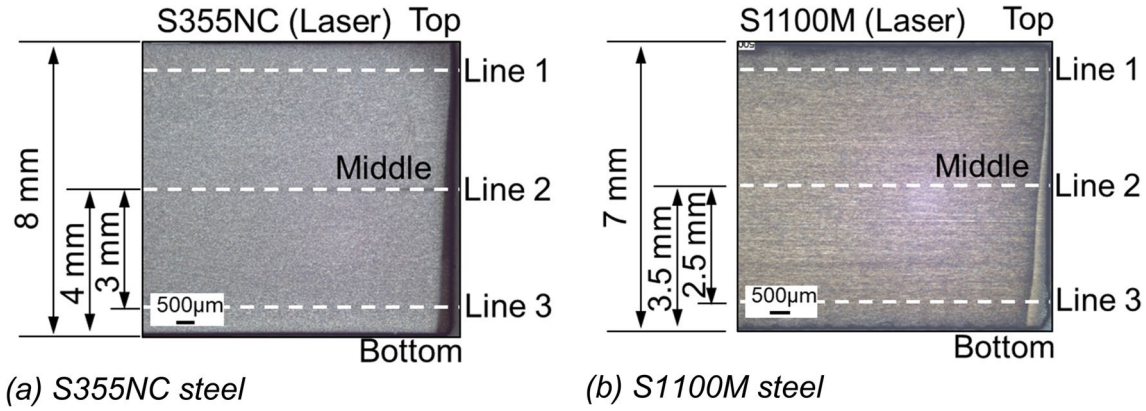

Fig. 7 Measured hardness along line 1, line 2, and line 3 on the half cross section of **a** S355NC and **b** S1100M steel

Fig. 8 Universal hardness testing machine ZHV30

is larger in plasma cutting (from protection gas) than in laser cutting as described in Section 2.2 (see Fig. 3).

4.2 Magnitude and distribution of cut-edge hardness

Referring to the description in Section 2.3, the HAZ of cut samples of S355 steel consists of CGHAZ, FGHAZ, and ICHAZ, while that of S1100 steel comprises CGHAZ, FGHAZ, ICHAZ, and SCHAZ. This is because the parent phase of S355 base steel is ferrite-pearlite, while that of S1100 base steel is auto-tempered martensite as seen in Fig. 9.

4.2.1 Vickers hardness test load

Figure 13 displays the measured magnitude and distribution of hardness along line 2 in cases of group A in Table 7. Figure 13 a shows that the measured magnitude of hardness in the HAZ of case 5-A is obviously smaller than those of cases 2-A to 4-A. This is because the width of HAZ created by thermal cutting is very narrow. Furthermore, the Vickers hardness test load affects the size of indentation, which influences the phase fractions in this area of indentation in the narrow HAZ (see Fig. 2). According to the above analysis as in Fig. 9a, the microstructure in CGHAZ and FGHAZ is the mixture of martensite and retained initial phase (ferrite-pearlite), while the phase fraction of ferrite-pearlite is small overall. With the increase of Vickers hardness test load resulting in the increased size of indentation, the percentage of the soft phase (ferrite-pearlite) at this area of indentation increases. Therefore, the measured hardness in the HAZ of case 5-A with the higher load (10 kgf) is lower compared to that, e.g., of case 3-A with the lower load (1 kgf) in Vickers tests. Besides, through careful observation in Fig. 13a, it can be found that the difference in the measured hardness at the same location in the HAZ of case 3 and case 5 becomes small when the location of measurement is close to the cut edge because that part of the initial phase transfers to martensite in ICHAZ (see Section 2.3), while most of the initial phase converts to martensite in CGHAZ and FGHAZ. Furthermore, ICHAZ is near BM. Therefore, the influence of the variation in the Vickers test load on the magnitude of hardness becomes weak close to BM. In Fig. 13a, the magnitude of hardness in cases 1-A, 2-A, 3-A, and 4-A are nearly the same overall although the distribution

Table 7 Experimental plan

	Experimental cases		Materials	Cutting method	Vickers hardness test load
Group A	Group A.1	Case 1-A	S355NC	Laser	HV0.1
		Case 2-A			HV0.5
		Case 3-A			HV1
		Case 4-A			HV5
		Case 5-A			HV10
	Group A.2	Case I-A	S1100M	Laser	HV0.1
		Case II-A			HV0.5
		Case III-A			HV1
		Case IV-A			HV5
		Case V-A			HV10
Group B	Group B.1	Case 1-B	S355NC	Laser	HV1
		Case 2-B		Plasma	
		Case 3-B		Milling	
	Group B.2	Case I-B	S1100M	Laser	HV1
		Case II-B		Plasma	
		Case III-B		Milling	

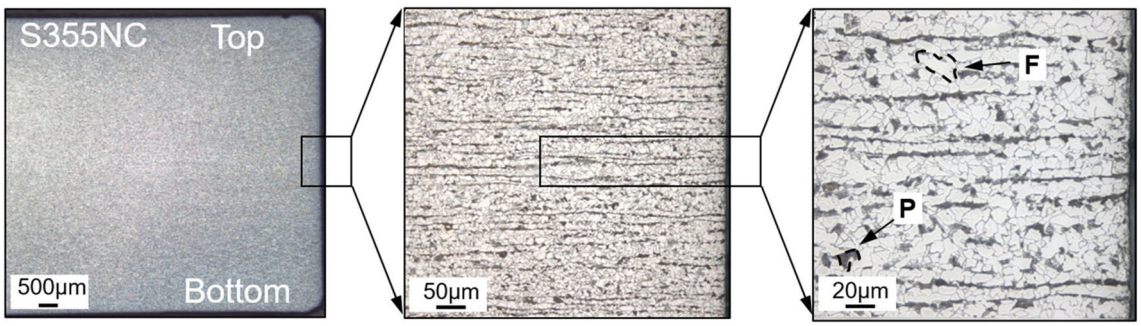

(a) S355NC (F: ferrite; P: pearlite)

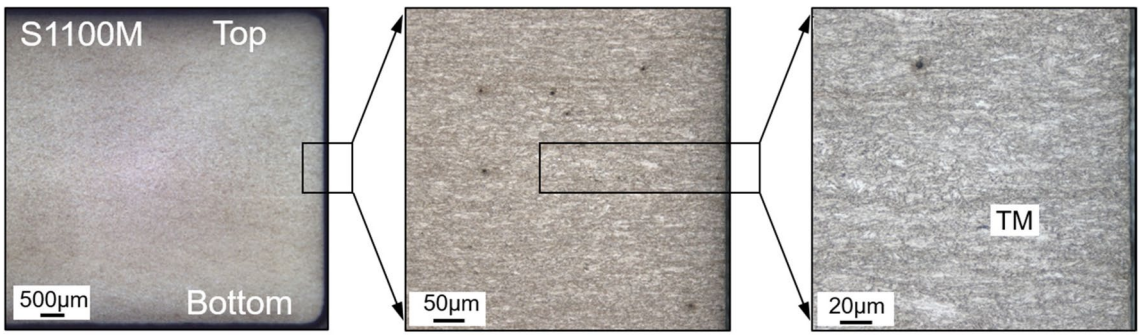

(b) S1100M (TM: tempered martensite)

Fig. 9 Macro- and micrographs of mechanically cut specimens of **a** S355NC (F ferrite, P pearlite) and **b** S1100M (TM tempered martensite)

of hardness along line 2 in case 1-A is not smooth. From Fig. 13a, it can be found that independent of the Vickers hardness test load, the measurements of hardness in the BM of case 1-A, case 2-A, case 3-A, case 4-A, and case 5-A are uniform. This is because no solid-state phase transformation (SSPT) occurs in BM. The change in the Vickers test load has almost no influence on the phase fractions in the area of indentation at BM. Therefore, the variation in the Vickers

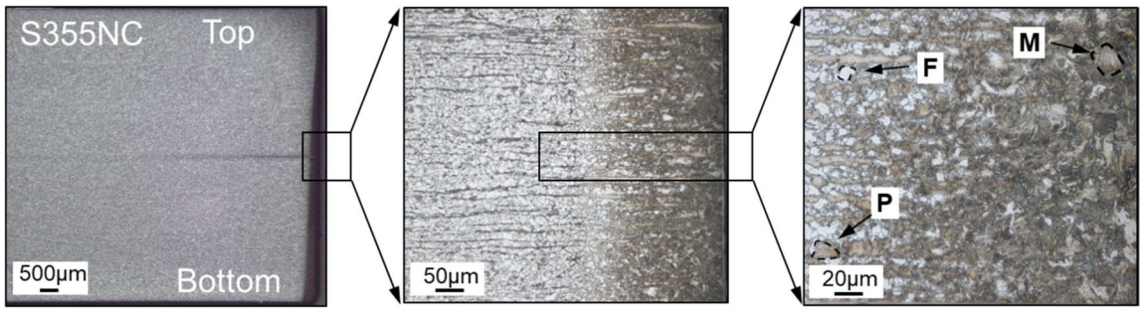

(a) S355NC (M: martensite; F: ferrite; P: pearlite)

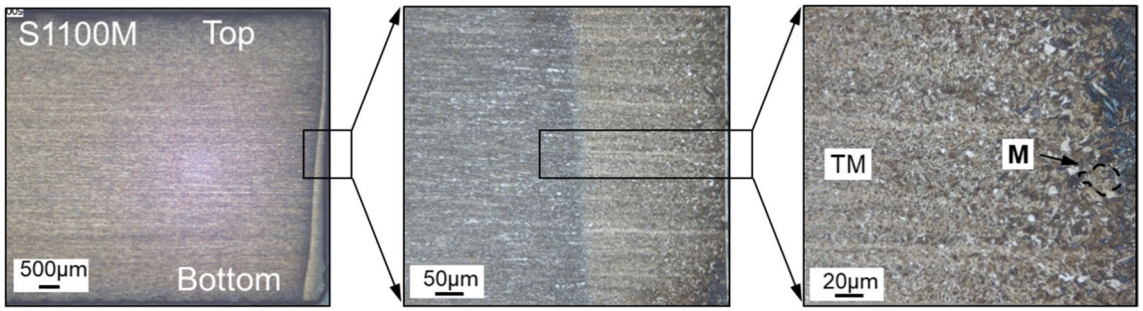

(b) S1100M (M: martensite; TM: tempered martensite)

Fig. 10 Macro- and micrographs of laser-cut specimens of **a** S355NC (M martensite, F ferrite, P pearlite) and **b** S1100M (M martensite, TM tempered martensite)

test load does not influence the measured magnitude of hardness in BM. Similar to Fig. 13a, the same phenomenon as described above can also be found in Fig. 13b. Nevertheless, the fluctuation of the measured hardness distribution along line 2 in the HAZ of case I-A (S1100M steel) is much stronger compared to that of case 1-A (S355NC steel). This is because the percentage of the retained initial phase in the HAZ of case I-A is higher than that of case 1-A as seen in Fig. 10. In Fig. 13b, the locations of the softened area in the HAZ of cases I-A, II-A, III-A, and IV-A are nearly the same, while that of case V-A is different.

4.2.2 Locations of hardness measurements

Figure 14 compares the measured magnitude and distribution of hardness along line 1, line 2, and line 3 in case 1-B and case I-B. From Fig. 14a, one can see that the distribution characteristics of hardness along lines 1–3 are almost co-identical. In the HAZ of the cut edge, the magnitude of hardness increases and remains nearly unchanged. The maximum hardness along these lines in Fig. 14a is nearly the same, which is about 450 HV1. Furthermore, the increased rate of hardness along lines 1–3 in ICHAZ is also almost the same. In Fig. 14a, the only difference in the measured hardness along lines 1–3 in case 1-B is the width of the hardness maximum. This is because the widths of HAZ along lines 1–3 in case 1-B are different as seen in Fig. 10a. The same phenomenon in Fig. 14a (S355NC steel) can also be found in Fig. 14b (S1100M steel).

4.2.3 Cutting processes

Figure 15 exhibits the measured magnitude and distribution of hardness along line 2 in cases of group B. From Fig. 15, it can be seen that the magnitude of hardness in the mechanically cut specimens is almost constant. Due to the use of the method, no HAZ exists as seen in Fig. 9. In Fig. 15, the mean value of hardness of base steel S355NC in case 3-B is about 153 HV1 and that of base steel S1100M in case III-B is around 379 HV1. In Fig. 15a, the magnitude and distribution of the hardness of the laser- and plasma-cut samples of S355NC are nearly the same, which are completely different from those of mechanically cut samples. This is because the microstructures in the HAZ of the laser- and plasma-cut specimens of S355NC steel are nearly the same as shown in Figs. 10a, and 11a. No matter what material it is, the same phenomenon from Fig. 15a (S355NC steel) can also be found in Fig. 15b (S1100M steel). There is no difference between the results of plasma or laser cutting methods used as primary energy source. Rather, the process parameter

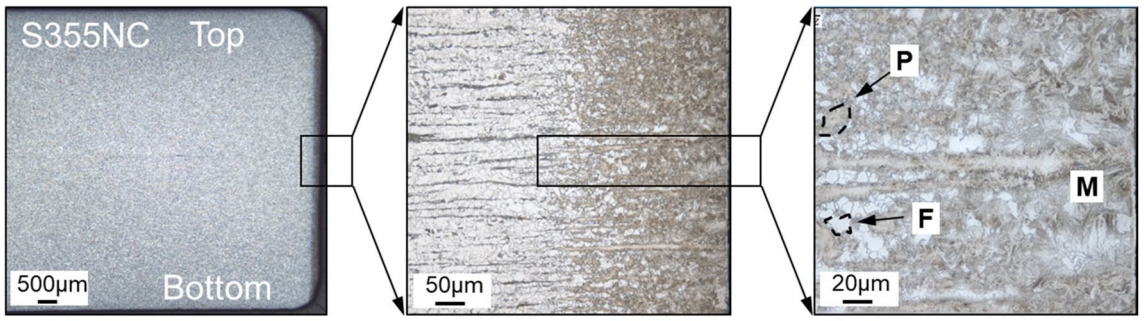

(a) S355NC (M: martensite; F: ferrite; P: pearlite)

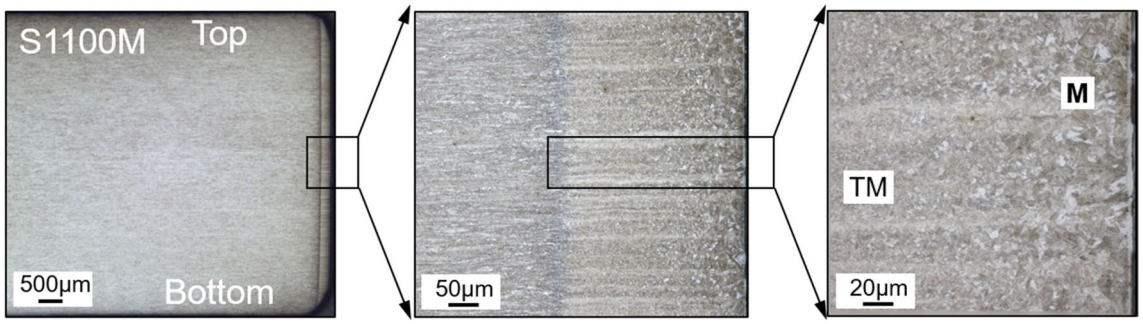

(b) S1100M (M: martensite; TM: tempered martensite)

Fig. 11 Macro- and micrographs of plasma-cut specimens of **a** S355NC (M martensite, F ferrite, P pearlite) and **b** S1100M (M martensite, TM tempered martensite)

cutting speed influences the duration of the local heat input. This also affects the cooling rate, which determines the microstructure and the hardness. The focus of the study is on the hardness method and on the comparison between cutting methods. In further studies, the influence of single parameters can be investigated.

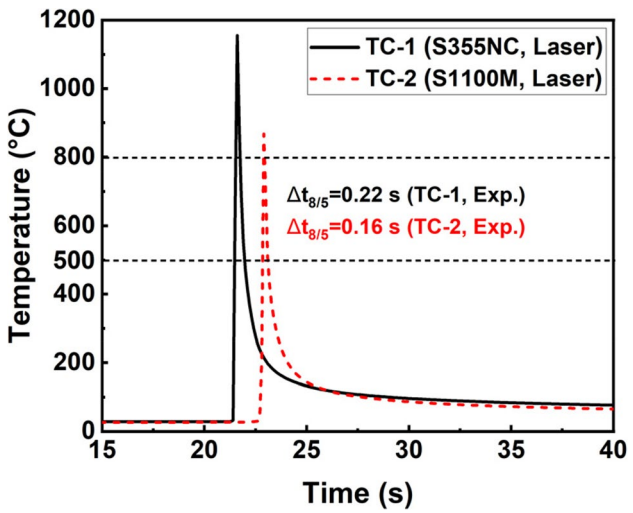

Fig. 12 Measured thermal cycles at TC-1 and TC-2 locations in laser-cut samples of steels S355NC and S1100M

5 Discussion

According to the described analysis, the Vickers test load obviously has an influence on the magnitude and distribution of hardness in the HAZ of thermally cut specimens of steels S355NC and S1100M. Consequently, the question arises as to which Vickers hardness test load is reasonable and should be applied in practice. To answer that question, it is necessary to illustrate that the aim for measuring hardness is to know the maximum value of hardness to assess the mechanical properties and to determine the location of the softened area with low hardness since failure easily starts at this region in high-strength steel specimens. Therefore, reliable measurements of hardness should display the accurate maximum value and the distribution to locate the softened area in HAZ. From Fig. 13, it can be concluded that independent of the steel grade, a Vickers hardness test load of 1 kgf or 0.5 kgf is the best choice, especially on cross sections without an angle < 10°, to expand the HAZ. To decrease the amount of indentations and the effort of the

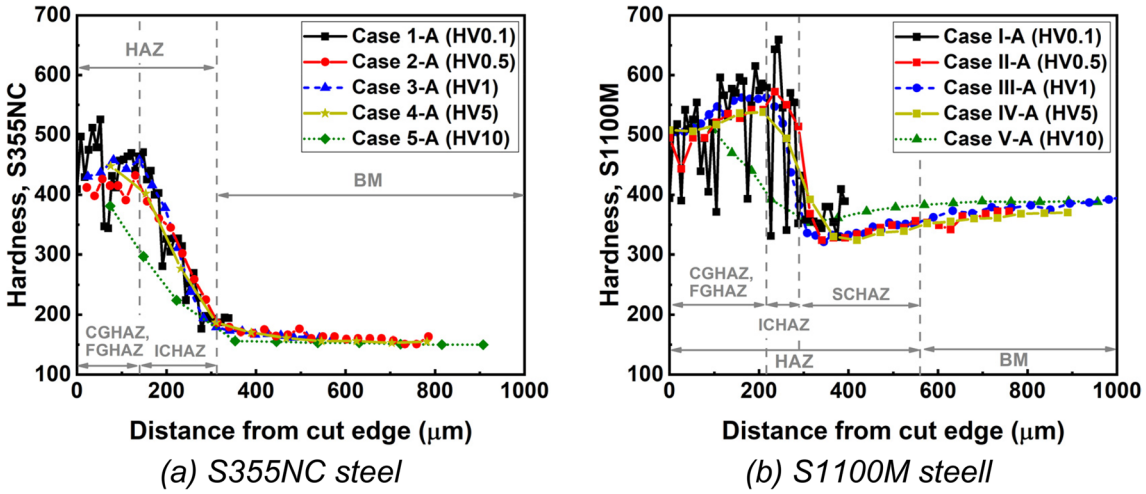

Fig. 13 Measured magnitude and distribution of hardness along line 2 for laser-cut samples of steels **a** S355NC and **b** S1100M

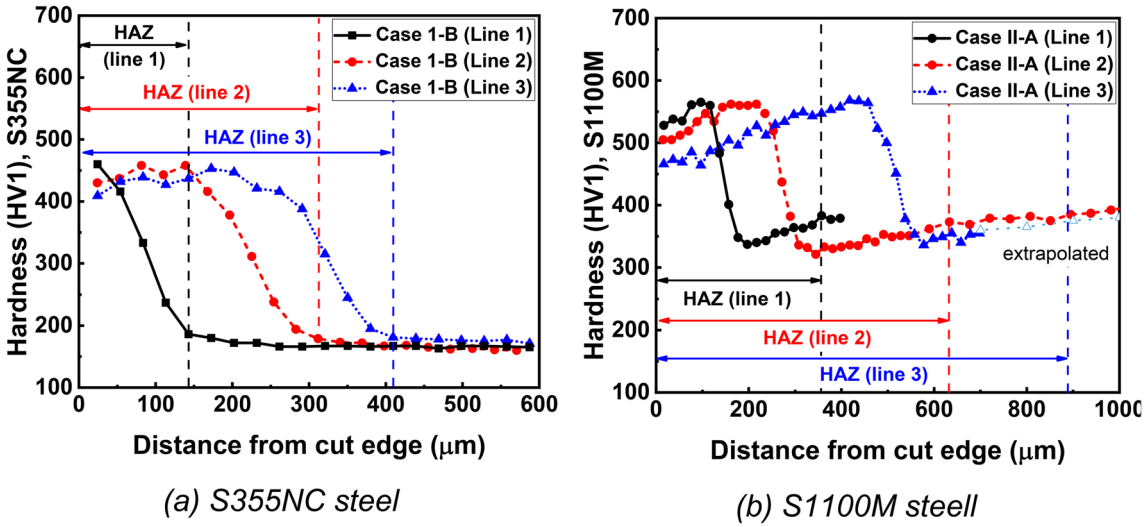

Fig. 14 Measured magnitude and distribution of hardness along lines 1–3 for laser-cut samples of steels **a** S355NC and **b** S1100M

experimental work, HV1 is recommended. Comparing to the measurements of hardness, the measured maximum hardness decreases if the Vickers test load is 5 kgf or higher. Nevertheless, the measured maximum hardness does change using an HV0.1 test load. Moreover, the distribution of hardness is not smooth, which could not show easily the location of the softened area in HAZ (SCHAZ) and the number of measurements for HV0.1 and also for HV0.5 is time-consuming. To be cost efficient, HV1 is finally recommended comparing the number of tests to make for HV0.5 and HV0.1 in consideration of the accuracy compared to HV5 and HV10. There is no negative impact on the environment of this research. The provided guidance to apply Vickers hardness testing method HV1 with a small angle at cut edges to widen the HAZ and to get reasonable results can be applied in practice and be considered for norms.

Based on the measurements of hardness as seen in Figs. 13, 14, and 15, one can see that the BM hardness of S355NC steel is about 153 HV1 and that of S1100M steel is about 379 HV1. Obviously, the hardness of S355NC BM is much lower compared to that of S1100M BM with a difference of about 200 HV1. This is because the parent phase of S355NC steel is ferrite-pearlite and that of S1100M steel is self-tempered martensite. Furthermore, the maximum hardness in the CGHAZ and FGHAZ of S355NC steel is about 450 HV1, while that of S1100M steel is about 550 HV1. Many works illuminated that the microhardness is determined by grain size, carbon content, phase, and phase

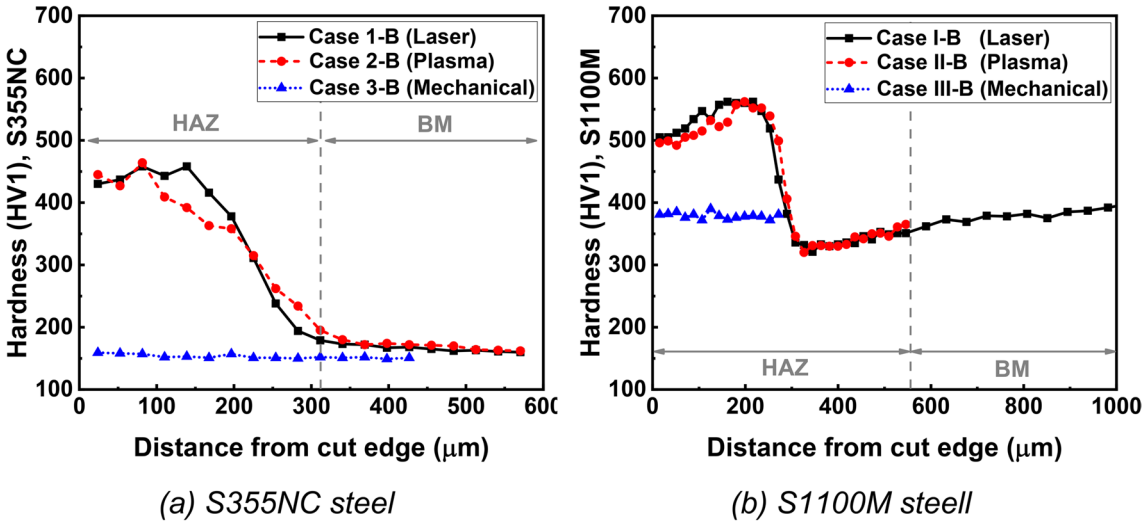

Fig. 15 Measured magnitude and distribution of hardness along line 2 for laser-, plasma-cut, and milled samples of steels **a** S355NC and **b** S1100M

fraction [31]. Based on the measured chemical compositions of steels S355NC and S1100M as seen in Tables 1 and 2, the different carbon contents and therefore the carbon equivalent (CET) of S1100M steel are about 0.44, which is higher than that of S355NC steel (0.291). Despite the similar martensite phase in HAZ, the maximum hardness of S1100M is higher compared to that of S355NC.

From Figs. 14 and 15, it can be found that the distribution characteristics of hardness in the HAZ of steels S355NC and S1100M are quite different. For better analysis, Fig. 16 is provided. From Fig. 16a, one can see that the value of hardness in the ICHAZ of S355NC steel increases from point a to point b due to the increasing fraction of the generated hard phase (martensite). Then, the hardness in the CGHAZ and FGHAZ of S355NC steel is nearly constant from point b to point c since the phase fraction becomes stable. In Fig. 16b, the hardness in the ICHAZ of S1100M steel also increases from point A to point B because of the generated hard phase (martensite). Nevertheless, the hardness in the CGHAZ and FGHAZ of S1100M steel decreases nearly linearly from point B to point C. A decreasing carbon content might be the reason. In fact, through careful observation of Figs. 15a and 16a, the maximum hardness in the HAZ of S355NC steel also decreases slightly closing to the cut edge. In Fig. 16b, the magnitude of hardness in SCHAZ decreases from point A to point D due to the tempering effect of the parent phase

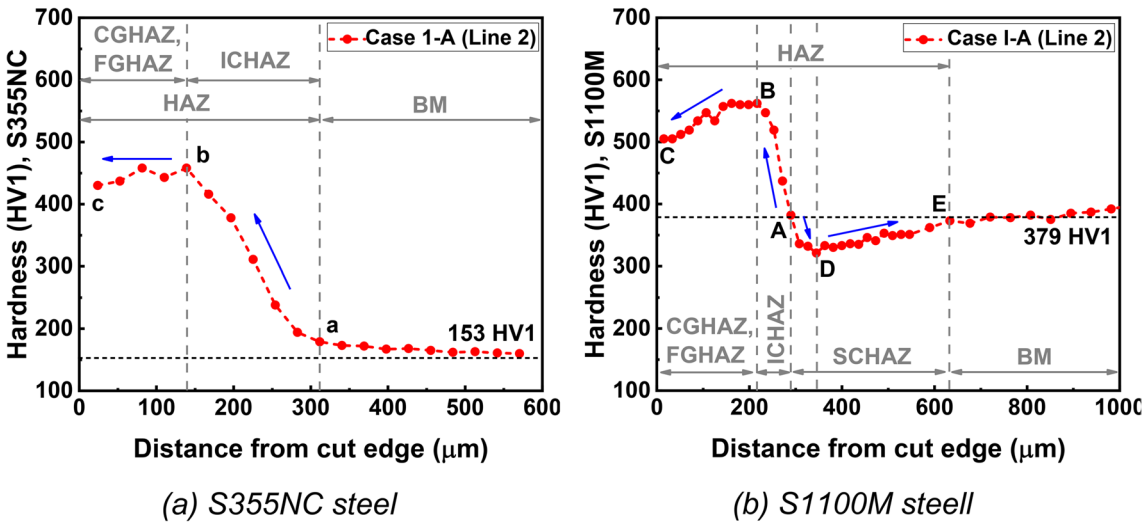

Fig. 16 Measured magnitude and distribution of hardness along line 2 for laser-cut samples of steels **a** S355NC and **b** S1100M

(self-tempered martensite). In essence, the microstructure of BM and SCHAZ is tempered martensite, while the tempering temperature and the endurance of tempering are different between BM and SCHAZ. Many research studies showed that the hardness decreases with tempering temperature overall [32]. From point D to point E, the magnitude of hardness increases due to the weakening tempering effect back to the level of the base material.

6 Conclusions

In the current work, the magnitude and distribution of hardness in thermally and mechanically cut specimens of steels S355 and S1100 were measured and compared. The experimental data indicates that:

- No HAZ is generated in the mechanically cut specimens, while the thermal cutting processes can generate HAZ at the cut edge.
- For structural steel, no matter what steel grade it is, it is recommended to measure hardness in the HAZ of thermally cut specimens by using 1 kgf as the Vickers test load.
- A cross section with an angle of about 5° is proven to be a good method to enlarge the HAZ to determine the hardness distribution at the cut edges.
- A guidance is provided to measure the hardness distribution of cut edges with reasonable effort in relation to the accuracy. The methodology is universal and can be applied for further investigations and in practice.
- The schematic hardness distributions of laser-cut specimens in the thickness direction are almost the same. However, the width of the high magnitude of hardness on the top surface is smaller than that on the bottom surface of laser-cut specimens of both steels S355 and S1100 due to the changing width of HAZ on the top surface and on the bottom surface.
- The magnitude and distribution of hardness in the laser- and plasma-cut samples are quite similar, which are obviously different compared to those of the mechanically cut specimens.
- The characteristic hardness distribution of the ultra-high-strength steel S1100 is different from that of the mild steel S355. A softened zone with lower hardness and a significant reduction of hardness adjacent to the cut edge can only be found in the thermally cut samples of S1100 steel.
- The maximum hardness in each phase of thermally cut samples of S1100 steel is higher than that of S355 steel.

Acknowledgements The authors are grateful to Mrs. K. Jehnert from Kjellberg as well as Mr. D. Mock and Mr. T. Kaiser from TRUMPF for their support in thermal cutting experiments.

Author contribution Paul Diekhoff: investigation, methodology, conceptualization, writing—review and editing; Jiamin Sun: conceptualization, writing—original draft, formal analysis, writing—review and editing; Thomas Nitschke-Pagel: formal analysis, writing—review and editing; Klaus Dilger: writing—review and editing.

Funding Open Access funding enabled and organized by Projekt DEAL. This study was financially supported by the Arbeitsgemeinschaft industrieller Forschungsvereinigungen (AiF) under project number 20937N, "Qualification of numerical simulations for the characterization and evolution of the boundary layer condition of free thermal interfaces."

Declarations

Competing interests The authors declare no competing interests.

References

1. European Committee for Standardization (CEN) (2004) EN 10025: hot rolled products of structural steels. European Standard, Brussels
2. U.S. Department of Energy's (DOE's) Vehicle Technologies Program (VTO) (2014) FY2013 lightweight materials R&D annual progress report. EERE Publication and Product Library
3. Khurshid M (2017) Static and fatigue analyses of welded steel structures – some aspects towards lightweight design. KTH-Royal Institute of Technology, Dissertation, Stockholm
4. Jimenez-Pena M, Goulas C, Rossi B, Debruyne D (2019) Influence of hole-making procedures on fatigue behavior of high strength steel plates. J Constr Steel Res 158:1–14
5. Belforte D, Buschow K, Robert W, Merton C, Bernard I, Edward J, Subhash M, Patrick V (2001) Laser Cutting. Encyclopedia of Materials: Science and Technology, Oxford, pp 4399–4402
6. Amraei M, Skriko T, Björk T, Zhao X (2016) Plastic strain characteristics of butt-welded ultra-high strength steel (UHSS). Thin-Walled Struct 109:227–241
7. Zubko P, Pesek L (2014) Correlation between hardness and fatigue properties. Key Eng Mater 662:197–200
8. Askeland D (1996) Polymers. The Science and Engineering of Materials, Springer, Boston, MA

9. Bauer B, Remenar M (2011) Thermal cutting welding engineering and technology / Kralj, Slobodan (ur.). Encyclopedia of Life Support Systems (EOLSS), Oxford, pp 1–35
10. Sokolov M, Salminen A, Kuznetsov M, Tsibulskiy I (2011) Laser welding and weld hardness analysis of thick section S355 structural steel. Mater Des 32:5127–5131
11. Dunder M, Wuherer T, Saardzic I, Maric D (2018) Analysis of heat-affected zone microstructures of steel P92 after welding and after post-weld heat treatment. J Adv Manuf Technol 102:3801–3812
12. Waterschoot T, Verbeken K, Cooman B (2006) Tempering kinetics of the martensitic phase in DP steel. ISIJ Int 46:138–146
13. Farabi N, Chen D, Li J, Zhou Y, Dong S (2010) Microstructure and mechanical properties of laser welded DP600 steel joints. Mater Sci Eng A 527:1215–1222
14. Boujelbene M, Alghamdi A, Miraoui I, Bayraktar E, Gazbar M (2017) Effects of the laser cutting parameters on the micro-hardness and on the heat affected zone of the mi-hardened steel. Int J Advances Appl Sci 4:19–25
15. Lazarevie A, Lazarevie D (2017) Investigations of material hardness and structural changes in the heat-affected zone during plasma cutting. Int J Advances Appl Sci 4:19–25
16. Diekhoff P, Hensel J, Nitschke-Pagel T, Dilger K, K. (2018) Investigation on reliable hardness measurements using the UCI method (ultrasonic contact impedance). Mater Test 9:833–840
17. Meyers M, Chawla K (2009) Material behavior of materials. Cambridge University Press, Cambridge
18. Esteban B (2017) Indentation hardness measurements at macro-, micro-, and nanoscale: a critical overview. Tribol Lett 65(23):1–18
19. Bauer B, Remenar M (2019) Welding engineering and technology – thermal cutting. In: Encyclopedia of life support systems, pp 1–38
20. Dudutis J, Pipiras J, Stonys R, Daknys E, Kilikevicius A, Kasparaitis A, Raciukaitis G, Gecys P (2020) In-depth comparison of conventional glass cutting technologies with laser-based methods by volumetric scribing using Bessel beam and rear-side machining. Opt Express 28:32133–32151
21. Caristan C (2014) Laser cutting guide for manufacturing. Society of Manufacturing Engineers, Michigan
22. Nemchinsky V (1998) Plasma flow in a nozzle during plasma arc cutting. J Phys 21:3102–3107
23. Schneider G (2002) Cutting tool applications. ASM International
24. Kömi J, Karjalainen P, Porter D (2016) Direct-quenched structural steels. Encyclopedia of iron, steel, and their alloys. Taylor & Francis, London
25. Francis J, Mazur W, Bhadeshia H (2006) Type IV cracking in ferritic power plant steels. Mater Sci Technol 22:1387–1395
26. Bhadeshia H, Honeycombe S (2006) Steels: microstructure and properties. Elsevier, Burlington
27. Diekhoff P, Hensel J, Nitschke-Pagel T, Dilger K (2020) Investigation on fatigue strength of cut edges produced by various cutting methods for high-strength steels. Weld World 64:545–561
28. Diekhoff P, Drebing J, Hensel J, Nitschke-Pagel T, Dilger K (2021) Influence of competing notches on the fatigue strength of cut plate edges. Weld World 65:1791–1803
29. Bursi O, D'Incau M, Zanon G, Raso S, Scardi R (2017) Laser and mechanical cutting effects on the cut-edge properties of steel S355N. J Constr Steel Res 133:181–191
30. Astakhov VP, Outeiro J (2019) Importance of temperature in metal cutting and its proper measurement/modeling. In: Davim J (ed) Measurement in machining and tribology, Materials forming, machining and tribology. Springer, Cham, pp 1–47
31. Weng S, Huang Y, Xuan F, Luo L (2015) Correlation between microstructure, hardness and corrosion ofwelded joints of disc rotors. Procedia Eng 130:1761–1769
32. Hu F, Wu KM, Hou TP, Shirzadi AA (2014) Effect of tempering temperature on the microstructure and hardness of a super-bainitic steel containing Co and Al. ISIJ Int 54:926–931